Optik - International Journal for Light and Electron Optics 225 (2021) 165820

Contents lists available at ScienceDirect

Optik - International Journal for Light and Electron Optics

journal homepage: www.elsevier.com/locate/ijleo

Original research article

Feasible and economical scheme to entangle a polarized coherent state and a polarized photon

Dat Thanh Le [a,b,*], Cao Thi Bich [c,d], Nguyen Ba An [b,d,**]

[a] ARC Centre for Engineered Quantum System, School of Mathematics and Physics, University of Queensland, Brisbane, QLD 4072, Australia
[b] Thang Long Institute of Mathematics and Applied Sciences (TIMAS), Thang Long University, Nghiem Xuan Yem, Hoang Mai, Hanoi 10000, Viet Nam
[c] Graduate University of Science and Technology, Vietnam Academy of Science and Technology (VAST), Hanoi 10000, Viet Nam
[d] Institute of Physics, Vietnam Academy of Science and Technology (VAST), 18 Hoang Quoc Viet, Cau Giay, Hanoi 10000, Viet Nam

ARTICLE INFO

Keywords:
Hybrid entanglement
Polarized coherent states
Decoherence effect
Realistic resources
Device imperfections

ABSTRACT

We design a scheme to generate a new type of hybrid entanglement between a macroscopic polarized coherent state and a single polarized photon. Concretely, a polarized Schrodinger cat state, an entangled polarized photon pair, and a polarized coherent state, which have been prepared off-line, are supplied as inputs to our scheme. Then, using conventional optical devices such as beam splitters, polarizing beam splitters, half-wave plates, and photon-number-resolving detectors, all the necessary operations can be effectively performed in-line. Conditioned on photon detection results, creation of the desired hybrid entanglement is heralded. The total success probability of our scheme is twice as high as that in existing schemes for unpolarized coherent states. Our scheme is not only feasible but also economical with regard to resource consumption because no active displacement operations must be utilized in-line. We also consider practical factors affecting the scheme performance, including decoherence of the input states, realistic resources, and device imperfections. Detailed analyses show that our scheme is robust against small imperfection effects and could be implemented with current technology. The proposed hybrid entanglement would serve as a vital resource for processing information encoded in superpositions of differently polarized coherent states which represent a new format of qubit.

1. Introduction

Hybrid approach, which simultaneously harnesses quantum systems of dissimilar natures, promises potential applications in quantum information processing and quantum computing within modern heterogeneous networks built on multiple physical platforms with distinct types of qubit encodings [1–4]. For instance, hybrid entanglement between microscopic and macroscopic systems [5–12] has been created to illustrate the renowned Schrodinger's thought experiment [13]. In the context of optical quantum information processing, hybrid approach generally combines discrete-variable (DV) and continuous-variable (CV) systems, each of which possesses their own pros and cons [14,15]. Concretely, implementation of CV systems and tools features in its determinism but suffers from less-than-one fidelities [16,17], while implementation of DV systems and tools is probabilistic yet with unit fidelities [16,17]. Hybridizing both CV and DV approaches on an appropriate footing would exploit advantages and, at

* Correspondence to: Thang Long Institute of Mathematics and Applied Sciences (TIMAS), Thang Long University, Nghiem Xuan Yem, Hoang Mai, Hanoi 10000, Viet Nam.
** Corresponding author.
E-mail addresses: thanhdat.le@uq.net.au (D.T. Le), annb@thanglong.edu.vn (N.B. An).

https://doi.org/10.1016/j.ijleo.2020.165820
Received 17 August 2020; Received in revised form 27 September 2020; Accepted 14 October 2020
Available online 22 October 2020

the same time, suppress downsides of each approach used separately [18]. Therefore, hybrid approach in general and in the optical domain in particular has been attracting great attention and remarkable progress in quantum communication [18–25] as well as in quantum computation [26–29] has been witnessed, paving the avenue for novel applications such as quantum metrology [6,30], Bell inequality verification [31,32], and demonstration of Einstein–Podolsky–Rosen steering [33].

Indispensable quantum channels to bridge across remote nodes of a DV–CV heterogeneous quantum network are DV–CV hybrid entangled states, whose generation schemes have been theoretically put forward and experimentally realized by several groups [18,23–25,34–42] . These DV–CV hybrid entangled states, in general, can be categorized into two types. The first type entangles a CV state and a single-rail photonic qubit in the form [18,23,24,37–40]

$$\frac{1}{\sqrt{2}}\left(|\mathrm{CV}_0\rangle_A|0\rangle_B + |\mathrm{CV}_1\rangle_A|1\rangle_B\right), \tag{1}$$

where $|\mathrm{CV}_0\rangle_A$ and $|\mathrm{CV}_1\rangle_A$ are two orthogonal (or nearly orthogonal) CV states belonging to node A, while $|0\rangle_B$ and $|1\rangle_B$ are respectively vacuum and single photon state of node B. Two typical examples of the above type of hybrid entanglement include $(|\alpha\rangle|0\rangle + |-\alpha\rangle|1\rangle)/\sqrt{2}$ where $|\pm\alpha\rangle$ are coherent states with amplitudes $\pm\alpha$ [37–39] and $(|\mathrm{cat}_\alpha^+\rangle|0\rangle + |\mathrm{cat}_\alpha^-\rangle|1\rangle)/\sqrt{2}$ where $|\mathrm{cat}_\alpha^\pm\rangle = N_\alpha^\pm(|\alpha\rangle \pm |-\alpha\rangle)$, with normalization factors $N_\alpha^\pm$, are even/odd Schrodinger cat states [18,23,24,40]. The second type of DV–CV hybrid entanglement appears between a CV state and a polarized photon [25,41,42]

$$\frac{1}{\sqrt{2}}\left(|\mathrm{CV}_0\rangle_A|H\rangle_B + |\mathrm{CV}_1\rangle_A|V\rangle_B\right), \tag{2}$$

where $|H\rangle$ ($|V\rangle$) represents state of a horizontally (vertically) polarized single photon. The hybrid entangled states (2), compared to those given by (1), could be more favorable for information processing owing to their polarization DV part. Specifically, a polarized qubit state, unlike that of a single-rail qubit, is definitely a one-photon state in which information is encoded over polarization degree of freedom (DoF), thus rendering it robust to losses and inefficient detections [25]. Moreover, single-qubit gates for polarized qubits are straightforwardly implemented using quarter-wave plates (QWPs) and half-wave plates (HWPs) [43,44], while those for single-rail qubits, which do not preserve photon number, are troublesome to realize [45]. The two above-mentioned types of hybrid entanglement have been thoroughly compared with regards to quantum teleportation [46,47]. Recently, an attempt to produce hybrid entanglement of the form

$$a|\mathrm{cat}_\alpha^+\rangle_A|H\rangle_B + b|\mathrm{cat}_\alpha^-\rangle_A|V\rangle_B, \tag{3}$$

with $|a|^2 + |b|^2 = 1$, has been made exploiting photon subtraction technique [25], but the actually generated state is mildly approximate to the ideal one, with the addition of a large vacuum component in the DV mode. Also, theoretical proposals to prepare hybrid entanglement of the form

$$\frac{1}{\sqrt{2}}\left(|\alpha\rangle_A|H\rangle_B + |-\alpha\rangle_A|V\rangle_B\right), \tag{4}$$

have been suggested in Refs. [41,42]. In these proposals, a small fraction of a Schrodinger cat state that is reflected from an unbalanced beam splitter (BS) is interfered on a balanced beam splitter (BBS) with a displaced mode of an entangled polarization photon pair. The interference erases “which-path” information while retains polarization information of the other mode of the entangled photon pair [42]. Under perfect conditions the schemes in Refs. [41,42] can create the hybrid entangled state of the form (4). However, in Refs. [41,42] the success probability is still quite low and use of displacement operators is required. Although displacement operation can be implemented in practice with the help of an additional intense laser and a highly transmissive BS [48], the practically displaced state is just an approximation to the desired theoretically displaced one, so unit fidelity cannot be achieved in principle.

In this paper, we propose a displacement-free scheme to create a new type of hybrid entanglement of a form similar to that defined in Eq. (4) but with the CV component being differently polarized coherent states, i.e., we aim at the state

$$|\Psi\rangle_{AB} = \frac{1}{\sqrt{2}}\left(|\alpha_H\rangle_A|H\rangle_B + |-\alpha_V\rangle_A|V\rangle_B\right), \tag{5}$$

where $|\pm\alpha_{H/V}\rangle$ are horizontally/vertically polarized coherent states with amplitudes $\pm\alpha$ [49]. The hybrid entangled state $|\Psi\rangle_{AB}$ connects two heterogeneous nodes: one working with the well-known DV qubit encoding $x|H\rangle + y|V\rangle$, with $|x|^2 + |y|^2 = 1$, and the other with a new type of CV qubit encoding

$$|q\rangle = \mathcal{N}(c|\alpha_H\rangle + d|-\alpha_V\rangle), \tag{6}$$

with $\mathcal{N} = [|c|^2 + |d|^2 + 2e^{-|\alpha|^2}\mathrm{Re}(cd^*)]^{-1/2}$. Note that Eq. (6) is a superposition of two coherent states that are distinguishable not only by opposite-in-sign amplitudes but also by sharply distinct polarizations. Such qubit encoding is different from the conventional qubit encodings $\propto c|\alpha\rangle + d|-\alpha\rangle$ [50] or $\propto c|\alpha_{H/V}\rangle + d|-\alpha_{H/V}\rangle$ [49] in which the two superposed coherent states are either unpolarized or of the same polarization. The new type of encoding in Eq. (6) could play its own role in quantum information processing, since one can exploit both the amplitude and the polarization DoF for readout and manipulation of the CV part. In fact, utilization of polarization DoF over coherent-state carriers has been applied in quantum key distribution protocols [51–54], which are shown to be robust against losses. Remarkably, as will be elucidated, exploiting polarized coherent states instead of unpolarized ones for generation of the hybrid entangled state (5) helps to avoid use of displacement operation and improves the above-mentioned limitations of the

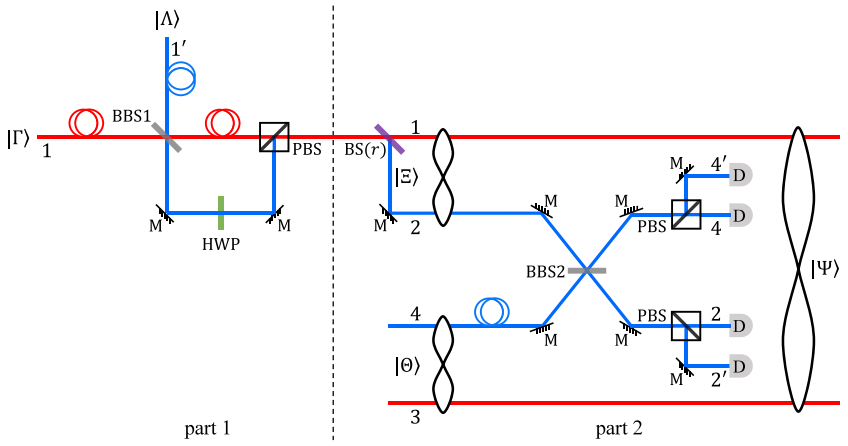

Fig. 1. (Color online) Scheme to generate the DV–CV hybrid entanglement between a polarized coherent state and a single polarized photon, involving two main parts. Part 1 prepares a polarized Schrodinger cat state in mode 1 given by Eq. (10). Part 2 performs joint manipulations and measurements on modes 2 and 4; depending on the measurement outcomes, modes 1 and 3 will be projected onto the desired hybrid entanglement. Here $|\Gamma\rangle \equiv |\Gamma\rangle_1$ defined in Eq. (7), $|\Lambda\rangle \equiv |\Lambda\rangle_{1'}$ defined in Eq. (8), and $|\Theta\rangle \equiv |\Theta\rangle_{34}$ defined in Eq. (9) are the needed inputs, $|\Xi\rangle \equiv |\Xi\rangle_{12}$ is a CV polarization entangled state given by Eq. (12), and $|\Psi\rangle \equiv |\Psi\rangle_{13}$ is the target prepared state given in Eq. (5). BS is short for beam splitter, BBS balanced beam splitter, PBS polarizing beam splitter, HWP half-wave plate, D photon-number-resolving detector, M mirror, and the delaying circles in paths 1, 1' and 4 can be adjusted to synchronize the time of incidence of modes on an optical device.

schemes in Refs. [41,42]. Namely, under the ideal conditions, in our scheme the total success probability doubles compared to that in Refs. [41,42] and the fidelity is exactly equal to one.

The structure of this paper is the following. In Section 2, we describe our scheme for generation of the target hybrid entangled state $|\Psi\rangle_{AB}$ as defined in Eq. (5). Necessary input states are specified, steps to proceed are detailed, and the total success probability is derived analytically in the same Section 2. We then in Section 3 analyze the scheme performance under practical circumstances; namely, we take into account the effect of decoherence of the input states and consider possible realistic resources as well as imperfect devices. Some discussions and conclusions are drawn in the final section, Section 4. Additionally, relevant appendices are included providing explicit calculations for the results in the main text.

2. Scheme details

Our scheme to entangle a polarized coherent state and a single polarized photon into the hybrid entanglement of the form (5) is visually illustrated in Fig. 1, consisting of two parts. In what follows, we present in detail the content and the purpose of each of these parts.

The required input states for the scheme include an horizontally polarized even Schrodinger cat state $|\Gamma\rangle_1$, a horizontally polarized coherent state $|\Lambda\rangle_{1'}$, and an entangled polarization photon pair $|\Theta\rangle_{34}$, which are respectively given by

$$|\Gamma\rangle_1 = N(\beta)\left(|\beta_H\rangle + |-\beta_H\rangle\right)_1, \tag{7}$$

$$|\Lambda\rangle_{1'} = |\beta_H\rangle_{1'}, \tag{8}$$

$$|\Theta\rangle_{34} = \frac{1}{\sqrt{2}}\left(|H\rangle_3|V\rangle_4 + |V\rangle_3|H\rangle_4\right), \tag{9}$$

where β is assumed to be real for simplicity and $N(\beta) = [2(1+e^{-2\beta^2})]^{-1/2}$ is a normalization factor.

Our scheme starts off by injecting $|\Gamma\rangle_1$ and $|\Lambda\rangle_{1'}$ respectively into path 1 and path 1′ of the first BBS (denoted by BBS1) in part 1 of the setup in Fig. 1. A HWP is placed on path 1′ after the BBS1 and the two modes along path 1 and path 1′ meet again at a polarizing beam splitter (PBS). Since the HWP transforms horizontal polarization to vertical one (and vice versa) while the PBS transmits horizontally polarized photons but reflects vertically polarized ones, it is straightforward to check that the output of part 1 is

$$|\Omega\rangle_1 = N(\beta)\left(|(\beta\sqrt{2})_H\rangle + |(-\beta\sqrt{2})_V\rangle\right)_1. \tag{10}$$

Here since $\langle\beta_H\ |-\beta_H\rangle = \left\langle(\beta\sqrt{2})_H\ |(-\beta\sqrt{2})_V\right\rangle = e^{-2\beta^2}$, both $|\Gamma\rangle_1$ and $|\Omega\rangle_1$ have the same normalization factor $N(\beta)$, despite their differences in amplitudes and polarizations. The state $|\Omega\rangle_1$, by means of a PBS, a HWP, and a phase shifter (PS), can be transformed into $N(\beta)\left(|(\beta\sqrt{2})_H\rangle_1|0\rangle_{1'} + |0\rangle_1|(\beta\sqrt{2})_H\rangle_{1'}\right)$, which is an infinite superposition of NOON states that are of great interest in quantum metrology applications [30,55]. Noteworthily, the state $|\Omega\rangle_1$ is a particular case of the new type of encoding in Eq. (6) with $c = d = 1$ and $\alpha = \beta\sqrt{2}$. Moreover, it turns out that the general new-type qubit state (6) with arbitrary coefficients c and d can be prepared

by the same part 1 in Fig. 1 with the input states $|\Gamma\rangle_1$ in Eq. (7) and $|\Lambda\rangle_{1'}$ in Eq. (8) replaced by $\mathcal{N}(c|(\alpha/\sqrt{2})_H\rangle + d|(-\alpha/\sqrt{2})_H\rangle)_1$ and $|(\alpha/\sqrt{2})_H\rangle_{1'}$, respectively.

The state $|\Omega\rangle_1$ outgoing from part 1 then enters part 2 of the setup where it is split by a general BS with reflectivity r (and transmissivity $t = 1 - r$). With the convention for the action of a general BS on a pair of coherent states,

$$\mathrm{BS}_{AB}|\alpha\rangle_A|\beta\rangle_B = |\alpha\sqrt{t} + \beta\sqrt{r}\rangle_A|\alpha\sqrt{r} - \beta\sqrt{t}\rangle_B, \tag{11}$$

the single-mode state $|\Omega\rangle_1$ is transformed into a two-mode entangled one

$$|\Xi\rangle_{12} = N(\beta)\left(|\delta_H\rangle_1|\gamma_H\rangle_2 + |-\delta_V\rangle_1|-\gamma_V\rangle_2\right), \tag{12}$$

with $\delta = \beta\sqrt{2t}$ and $\gamma = \beta\sqrt{2r}$. The state $|\Xi\rangle_{12}$ is characterized not only by coherent states' amplitudes but also by their polarizations and thus is different from the commonly used entangled coherent state $\propto (|\delta\rangle|\gamma\rangle + |-\delta\rangle|-\gamma\rangle)_{12}$ [50]. More precisely, the state $|\Xi\rangle_{12}$ contains CV polarization entanglement quantified via quantum Stokes parameters [56]. In passing, another CV entangled state also characterized by both coherent states' amplitudes and polarizations in the form $(|\mathrm{cat}^+_{\alpha,H}\rangle|\mathrm{cat}^-_{\alpha,V}\rangle - |\mathrm{cat}^-_{\alpha,H}\rangle|\mathrm{cat}^+_{\alpha,V}\rangle)/\sqrt{2}$, with $|\mathrm{cat}^\pm_{\alpha,H}\rangle$ ($|\mathrm{cat}^\pm_{\alpha,V}\rangle$) being horizontally (vertically) polarized Schrodinger even/odd cat states with amplitude α, has been considered in the context of entanglement duality [49].

Up to this point, the input state $|\Theta\rangle_{34}$ of Eq. (9) has not been used yet. Recalling the Fock-state representation of a coherent state with real amplitude x, $|x\rangle = \sum_{n=0}^{\infty} f_n(x)|n\rangle$ with the coefficient $f_n(x) = e^{-x^2/2}x^n/\sqrt{n!}$ featuring the photon-number (Poisson) distribution $f_n^2(x) = e^{-x^2}x^{2n}/n!$, the product state $|\Xi\rangle_{12}|\Theta\rangle_{34} \equiv |\Sigma\rangle_{1234}$ at the beginning of part 2 of the setup in Fig. 1 can be rearranged as $|\Sigma\rangle_{1234} \to |\Sigma\rangle_{1324} \equiv |\Sigma\rangle$:

$$|\Sigma\rangle = \frac{N(\beta)}{\sqrt{2}}\sum_{n=0}^{\infty}\left[f_n(\gamma)|\mathbf{1}\rangle_{13}|n_H\rangle_2|V\rangle_4 + f_n(\gamma)|\mathbf{2}\rangle_{13}|n_H\rangle_2|H\rangle_4 + f_n(-\gamma)|\mathbf{3}\rangle_{13}|n_V\rangle_2|V\rangle_4 + f_n(-\gamma)|\mathbf{4}\rangle_{13}|n_V\rangle_2|H\rangle_4\right], \tag{13}$$

where for convenience we have set $|\mathbf{1}\rangle_{13} = |\delta_H\rangle_1|H\rangle_3$, $|\mathbf{2}\rangle_{13} = |\delta_H\rangle_1|V\rangle_3$, $|\mathbf{3}\rangle_{13} = |-\delta_V\rangle_1|H\rangle_3$, and $|\mathbf{4}\rangle_{13} = |-\delta_V\rangle_1|V\rangle_3$ and $|n_H\rangle(|n_V\rangle)$ is a Fock state containing n horizontally (vertically) polarized photons. While modes 1 and 3 of the state $|\Sigma\rangle$ are left untouched, modes 2 and 4 are let be interfered at a BBS (denoted by BBS2 in Fig. 1). Since

$$\mathrm{BS}_{AB}|j\rangle_A|k\rangle_B = \sum_{p=0}^{j}\sum_{q=0}^{k} B^{j,k}_{p,q}(r,t)|j-p+q\rangle_A|k-q+p\rangle_B, \tag{14}$$

with

$$B^{j,k}_{p,q}(r,t) = \left(C^p_j C^q_k C^p_{k-q+p} C^q_{j-p+q} t^{j+k-p-q} r^{p+q}\right)^{1/2}(-1)^{k-q}, \tag{15}$$

after the BBS2 the state $|\Sigma\rangle_{1324} \equiv |\Sigma\rangle$ in Eq. (13) becomes $|\Sigma'\rangle_{1324} \equiv |\Sigma'\rangle$:

$$|\Sigma'\rangle = \frac{N(\beta)f_1(\gamma)}{2}\left[\frac{(|\mathbf{1}\rangle + |\mathbf{4}\rangle)_{13}}{\sqrt{2}}(|1_V\rangle_2|1_H\rangle_4 - |1_H\rangle_2|1_V\rangle_4) + \frac{(|\mathbf{1}\rangle - |\mathbf{4}\rangle)_{13}}{\sqrt{2}}(|1_H\rangle_2|1_V\rangle_2 - |1_H\rangle_4|1_V\rangle_4)\right.$$
$$\left. + |\mathbf{2}\rangle_{13}(|2_H\rangle_2 - |2_H\rangle_4) - |\mathbf{3}\rangle_{13}(|2_V\rangle_2 - |2_V\rangle_4)\right] + \mathrm{OT}. \tag{16}$$

In Eq. (16) only terms with $n = 1$ are explicitly written, while terms with $n \neq 1$ are absorbed in "OT" (short for "other terms"). It can be verified that all the terms in "OT" do not contribute to the success of the scheme. Next, to obtain the desired state $|\Psi\rangle_{13}$ of the form (5) we measure modes 2 and 4 to figure out not only their photon numbers but also their polarizations. We can see intuitively from Eq. (16) that there are 5 situations.

Situation 0: if mode 2 or mode 4 each is found to contain two photons with the same polarization, then modes 1 and 3 will be projected onto a product state $|\mathbf{2}\rangle_{13} \equiv |\delta_H\rangle_1|V\rangle_3$ or $|\mathbf{3}\rangle_{13} \equiv |-\delta_V\rangle_1|H\rangle_4$, implying the failure to generate the target hybrid entangled state.

Situation 1: if mode 2 is found to contain one photon with vertical polarization and mode 4 is found to contain one photon with horizontal polarization, then modes 1 and 3 in the state $|\Sigma'\rangle$ will be collapsed into

$$\frac{(|\mathbf{1}\rangle + |\mathbf{4}\rangle)_{13}}{\sqrt{2}} \equiv \frac{1}{\sqrt{2}}\left(|\delta_H\rangle_1|H\rangle_3 + |-\delta_V\rangle_1|V\rangle_3\right). \tag{17}$$

Such state is nothing but the desired hybrid entanglement $|\Psi\rangle_{13}$ in Eq. (5) with amplitude

$$\alpha = \delta \equiv \beta\sqrt{2t}. \tag{18}$$

Situation 2: if mode 2 is found to contain one photon with horizontal polarization and mode 4 is found to contain one photon with vertical polarization, then modes 1 and 3 in the state $|\Sigma'\rangle$ will also be collapsed into the state (17).

Situation 3: if mode 2 is found to contain two photons with different polarizations, then the collapsed state will be

$$\frac{(|\mathbf{1}\rangle - |\mathbf{4}\rangle)_{13}}{\sqrt{2}} \equiv \frac{1}{\sqrt{2}}\left(|\delta_H\rangle_1|H\rangle_3 - |-\delta_V\rangle_1|V\rangle_3\right), \tag{19}$$

implying another successful event because the above state can be unitarily transformed to the state (17).

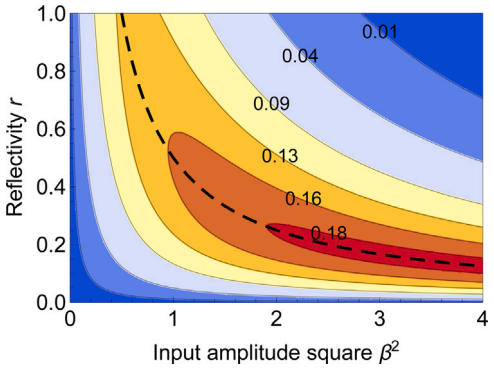

Fig. 2. (Color online) Total success probability of the scheme $P_T = 4P$ with P given in Eq. (24) as a function of the input amplitude square β^2 and the reflectivity r. The (black) dashed line represents the optimal reflectivity, $r^{\text{peak}} = 1/(2\beta^2)$, optimizing the total success probability P_T for $\beta^2 > 1/2$. Selected contour values for P_T are marked.

Situation 4: if mode 4 is found to contain two photons with different polarizations, then the collapsed state will be nothing else but the state (19).

To observe both photon number and polarization of the modes of interest, two PBSs and four photodetectors are arranged behind the BBS2 as seen in part 2 of the setup in Fig. 1. The successful event in Situation 1 is associated with the outcome of a projective measurement specified by the operator

$$\Pi_1 = |0\rangle_2\langle 0| \otimes |1\rangle_{2'}\langle 1| \otimes |1\rangle_4\langle 1| \otimes |0\rangle_{4'}\langle 0|, \tag{20}$$

and happens when the detectors $D_{2'}$ and D_4 each register one photon. Similarly, the other three successful Situations 2, 3, and 4 are associated with the projective measurements specified respectively by the operators

$$\Pi_2 = |1\rangle_2\langle 1| \otimes |0\rangle_{2'}\langle 0| \otimes |0\rangle_4\langle 0| \otimes |1\rangle_{4'}\langle 1|, \tag{21}$$

$$\Pi_3 = |1\rangle_2\langle 1| \otimes |1\rangle_{2'}\langle 1| \otimes |0\rangle_4\langle 0| \otimes |0\rangle_{4'}\langle 0|, \tag{22}$$

$$\Pi_4 = |0\rangle_2\langle 0| \otimes |0\rangle_{2'}\langle 0| \otimes |1\rangle_4\langle 1| \otimes |1\rangle_{4'}\langle 1|. \tag{23}$$

It is straightforward to check that the failure events in Situation 0 are excluded by the projective measurements specified by the above operators $\{\Pi_j; j = 1, 2, 3, 4\}$ and each of the four successful events in Situations 1, 2, 3, and 4 occurs with an equal probability

$$P = \langle \Sigma' | \Pi_{1(2,3,4)} | \Sigma' \rangle = \frac{N^2(\beta) f_1^2(\gamma)}{4} = \frac{r\beta^2 e^{-2r\beta^2}}{4(1 + e^{-2\beta^2})}. \tag{24}$$

Therefore, the total success probability of our scheme is $P_T = 4P$, which is twice as high as that reported in Refs. [41,42] where the coherent states are either unpolarized or of the same polarization.

The total success probability $P_T = 4P$, with P given in Eq. (24), is plotted in Fig. 2 as a function of β^2 and r. For $\beta^2 \leq 0.5$, the probability P_T increases monotonically with increasing r. For $\beta^2 > 0.5$, as $r\beta^2 \exp(-2r\beta^2)$ peaks at $2r\beta^2 = 1$, the probability P_T peaks at $r = r^{\text{peak}} = 1/(2\beta^2)$ which is displayed as a (black) dashed line in Fig. 2. This in turn yields $P_T^{\text{peak}} = 1/\left[2e(1 + e^{-2\beta^2})\right]$ approaching $1/(2e)$ for large β^2. Specifically, for $\beta^2 = \{2, 3, 4, \ldots\}$ corresponding to $r^{\text{peak}} = \{1/4, 1/6, 1/8, \ldots\}$ (i.e., $t^{\text{peak}} = \{3/4, 5/6, 7/8, \ldots\}$), the desired hybrid entangled state $|\Psi\rangle_{13}$ with good amplitudes $\alpha = \{1.732, 2.236, 2.646, \ldots\}$ is obtained with optimal total success probabilities $P_T^{\text{peak}} = \{18.063\%, 18.348\%, 18.388\%, \ldots\}$.

Before considering possible imperfect conditions that may be encountered in practice we note that the polarizations of the input states (7) and (8) can also be chosen to be vertical. In this case our scheme would generate a state of the form (5) but with the polarizations of the two coherent-state components to be exchanged, which is equally useful. The trick is that both the input states (7) and (8) should have the same polarization (i.e., they must be either horizontally or vertically polarized).

3. Decoherence effect, realistic resources, and device imperfections

Towards an implementation of our proposed scheme considerations of several practical issues should be paid attention to. Firstly, quality of the input states could be degraded at the moment of their utilization due to the decoherence effect caused by their interaction with the surrounding environments. Secondly, production of the genuine input states themselves is usually very hard and can thus be approximated by some other resources that are easier to prepare in practice. Thirdly, the optical devices used in our scheme, despite being readily available in the lab, may still suffer from certain imperfections, e.g., a BBS could be slightly unbalanced or a photodetector could be not 100% efficient. In the forthcoming subsections, we sequentially take into account the above-mentioned practical factors evaluating their influence on the success probability of the scheme and on the fidelity of the prepared state compared to those under ideal conditions.

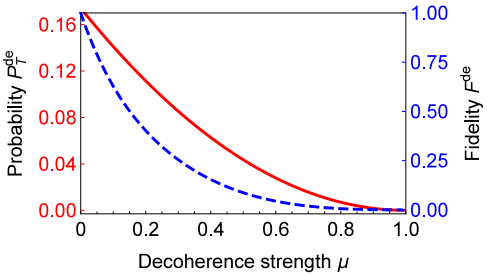

Fig. 3. (Color online) Total success probability P_T^{de} (solid line) and fidelity F^{de} (dashed line) given in Eqs. (31) and (32), respectively, as functions of the decoherence strength μ defined in Eq. (33). Here to generate the plot we choose the input amplitude $\beta = 1.2$ and the corresponding optimal reflectivity $r^{peak} \approx 0.347$.

3.1. Decoherence of the input states

The decoherence process we are interested in is photon loss, which is modeled by the master equation

$$\frac{d\rho}{d\tau} = \hat{D}\rho, \tag{25}$$

where ρ is the density operator of the total input state, τ denotes time, and $\hat{D}$ is the Linblad superoperator acting on ρ as $\hat{D}\rho = (\kappa/2)\sum_j (2a_j\rho a_j^\dagger - \rho a_j^\dagger a_j - a_j^\dagger a_j \rho)$. Here the subscript j indexes all the modes present in ρ, a_j ($a_j^\dagger$) is the annihilation (creation) operator of mode j, and κ is the decay rate which for simplicity has been assumed to be identical for all the modes. Initially, at $\tau = 0$ the input density operator ρ is

$$\rho(0) = |\Gamma\rangle_1\langle\Gamma| \otimes |\Lambda\rangle_{1'}\langle\Lambda| \otimes |\Theta\rangle_{34}\langle\Theta|, \tag{26}$$

where $|\Gamma\rangle_1, |\Lambda\rangle_{1'}$, and $|\Theta\rangle_{34}$ are respectively defined in Eqs. (7) - (9). Before arriving at the setup, the three inputs supposedly interacted with their environments for some time τ and experienced photon loss. The actual input density operator ρ then depends on the interaction time τ and the decay rate κ. Formally the time-dependent input density operator $\rho(\tau)$ can be written in the form $\rho(\tau) = e^{\hat{D}\tau}\rho(0)$ and using the results in Refs. [21,57] it is explicitly given by

$$\rho(\tau) = \rho_1(\tau) \otimes \rho_{1'}(\tau) \otimes \rho_{34}(\tau), \tag{27}$$

where

$$\rho_1(\tau) = N^2(\beta)\left[\,|\lambda_H\rangle_1\langle\lambda_H| + C_1|\lambda_H\rangle_1\langle-\lambda_H| + C_1|-\lambda_H\rangle_1\langle\lambda_H| + |-\lambda_H\rangle_1\langle-\lambda_H|\,\right], \tag{28}$$

$$\rho_{1'}(\tau) = |\lambda_H\rangle_{1'}\langle\lambda_H|, \tag{29}$$

$$\rho_{34}(\tau) = \frac{1}{2}\left[\rho_{3H}(\tau) \otimes \rho_{4V}(\tau) + \rho_{3V}(\tau) \otimes \rho_{4H}(\tau) + \nu^2(|H\rangle_3\langle V| \otimes |V\rangle_4\langle H| + |V\rangle_3\langle H| \otimes |H\rangle_4\langle V|)\right], \tag{30}$$

with $\lambda = \beta\nu$, $C_1 = \langle -\beta|\beta\rangle^{1-\nu^2}$, $\nu = e^{-\kappa\tau/2}$, and $\rho_{jK}(\tau) = \nu^2|K\rangle_j\langle K| + (1-\nu^2)|0\rangle_j\langle 0|$ for $j = 3, 4$ and $K = H, V$.

Repeating calculations in Section 2 with the decohered inputs in Eqs. (28)–(30) yields the following total success probability and fidelity under the effect of decoherence

$$P_T^{de} = \nu^2 P_T, \tag{31}$$

$$F^{de} = \frac{1}{2}\nu^2|\langle\alpha|\alpha\nu\rangle|^2(1 + C_1), \tag{32}$$

where P_T is defined below Eq. (24) and α is given in Eq. (18). A quick check for $\tau = 0$ (for which $\nu = C_1 = 1$) gives $P_T^{de} = P_T$ and $F^{de} = 1$, recovering the results obtained in Section 2 without the decoherence effect. This is a should-be fact, since $\tau = 0$ means that the input states did not interact with their environments (i.e., there is no decoherence). Let us define a new notation μ as

$$\mu = 1 - \nu \equiv 1 - e^{-\kappa\tau/2} \in [0, 1], \tag{33}$$

which represents the decoherence strength: $\mu = 0$ for $\tau = 0$ and $\mu = 1$ for $\tau = \infty$. In Fig. 3 we plot the total success probability P_T^{de} (solid line) and the fidelity F^{de} (dashed line) versus the decoherence strength μ. Roughly speaking, P_T^{de} and F^{de} degrade severely with increasing μ. For $\mu \geq 0.8$, both P_T^{de} and F^{de} almost vanish. This is understandable, since in this case the input states in Eqs. (28)–(30) are getting more and more decohered (even becoming almost completely vacuum for $\mu \to 1$), thus making the scheme performance worse and worse. However, it can be seen that P_T^{de} is seemingly less susceptible to μ than F^{de}. Discretely, when μ from 0 reaches 0.2, P_T^{de} reduces from over 0.16 to around 0.11, losing about 31% of its initial value, whereas F^{de} witnesses roughly 60% degradation decreasing from 1 to around 0.4. Quite acceptable total success probability and fidelity can be retained for a weak enough strength of decoherence: at $\mu = 0.01$ we have $P_T^{de} \approx 0.17$ and $F^{de} \approx 0.95$.

3.2. Realistic input resources

We emphasize that our scheme works not only for the input even cat state $|\Gamma\rangle_1$ in Eq. (7) but also for an odd cat one and which type of cat states to be used would result in distinct success probability and fidelity. Precise generation of these cat states in general is a daunting task; in most practical experiments, they are replaced with squeezed resources. Specifically, for small amplitudes even and odd cats can be very well approximated respectively by a squeezed vacuum and a squeezed single photon. While the former state can be generated deterministically via vacuum squeezing [58], production of the latter typically involves subtracting one photon which is of probabilistic nature and of low efficiency [59,60]. In that sense, approximate even cat states would be more experimentally accessible than approximate odd ones. In the Fock-state basis, the squeezed vacuum state $|\mathrm{sv}\rangle$ and the squeezed single photon state $|\mathrm{ss}\rangle$ are respectively of the forms

$$|\mathrm{sv}\rangle = \sum_{n=0}^{\infty} \frac{(-\tanh s)^n}{(\cosh s)^{1/2}} \frac{\sqrt{(2n)!}}{2^n n!} |2n\rangle, \tag{34}$$

$$|\mathrm{ss}\rangle = \sum_{n=0}^{\infty} \frac{(\tanh s)^n}{(\cosh s)^{3/2}} \frac{\sqrt{(2n+1)!}}{2^n n!} |2n+1\rangle, \tag{35}$$

where in both equations s is the squeezing parameter which is assumed to be real. The fidelity between the squeezed vacuum state $|\mathrm{sv}\rangle$ and the ideal even cat state of amplitude β is given by [61]

$$F^{\text{sv-even}} = \frac{2e^{-\beta^2(\tanh s+1)}}{(1+e^{-2\beta^2})\cosh s}, \tag{36}$$

whereas that between the squeezed single photon state $|\mathrm{ss}\rangle$ and the ideal odd cat state of amplitude β is [62]

$$F^{\text{ss-odd}} = \frac{2\beta^2 e^{\beta^2(\tanh s-1)}}{(1-e^{-2\beta^2})(\cosh s)^3}. \tag{37}$$

Fixing β, we find s that optimizes $F^{\text{sv-even}}$ and $F^{\text{ss-odd}}$ respectively as $s^{\text{opt}}_{\text{even}} = -\operatorname{arcsinh}(2\beta^2)/2$ and $s^{\text{opt}}_{\text{odd}} = \operatorname{arcsinh}(2\beta^2/3)/2$. Substituting these optimal values of s into Eqs. (36) and (37), we find that for small values of β ($\lesssim 1$) the two fidelities $F^{\text{sv- even}}$ and $F^{\text{ss-odd}}$ can be very high. For instance, for $\beta = 0.7$ we have $F^{\text{sv-even}} \approx 0.9934$ when $s = -0.43358$ and $F^{\text{ss-odd}} \approx 0.9998$ when $s = 0.16056$.

Besides the cat states, the entangled polarization photon pair $|\Theta\rangle_{34}$ in Eq. (9) is also a requisite input state in our scheme. In practice, the state $|\Theta\rangle_{34}$ is routinely generated via the type-II spontaneous parametric down conversion (SPDC) process, in which a single mother optical pumping beam creates two daughter photon beams (signal and idler) which are entangled in orthogonal polarizations [63]. The output state $|\mathrm{SPDC}\rangle$ of such SPDC process unavoidably includes a large vacuum component and is approximately given by [44]

$$|\mathrm{SPDC}\rangle_{34} \simeq \sqrt{1-\lambda^2}|0\rangle_3|0\rangle_4 + \lambda|\Theta\rangle_{34} + \mathrm{O}(\lambda^2), \tag{38}$$

where λ is the (dimensionless) SPDC interaction strength typically of order 10^{-2}.

In this subsection, we analyze the scheme performance when using either the squeezed vacuum state $|\mathrm{sv}\rangle$ or the squeezed single photon state $|\mathrm{ss}\rangle$ in Eqs. (34) and (35) as a possible realistic input state for mode 1 and the SPDC output state $|\mathrm{SPDC}\rangle_{34}$ in Eq. (38) as a possible realistic input state for modes 3 and 4. As a result of using such realistic input resources, expressions of the total success probability P_T^{re} and the fidelity F^{re} are derived as

$$P_T^{\text{re}} = (1-\lambda^2)P_{T,0}^{\text{re}} + \lambda^2 P_{T,\Theta}^{\text{re}}, \tag{39}$$

$$F^{\text{re}} = \frac{(1-\lambda^2)P_{T,0}^{\text{re}}F_0^{\text{re}} + \lambda^2 P_{T,\Theta}^{\text{re}}F_\Theta^{\text{re}}}{P_T^{\text{re}}} = \frac{\lambda^2 P_{T,\Theta}^{\text{re}}}{P_T^{\text{re}}}F_\Theta^{\text{re}}, \tag{40}$$

where $P_{T,0}^{\text{re}}$ and F_0^{re} ($P_{T,\Theta}^{\text{re}}$ and F_Θ^{re}) are the total success probability and the fidelity when the initial input state of modes 3 and 4 is solely vacuum (the entangled polarization photon pair $|\Theta\rangle_{34}$). The expression for the total success probability P_T^{re} in Eq. (39) is interpreted as the sum of $P_{T,0}^{\text{re}}$ and $P_{T,\Theta}^{\text{re}}$ weighted respectively by the populations of vacuum and the state $|\Theta\rangle_{34}$ in the state $|\mathrm{SPDC}\rangle_{34}$. As for the fidelity F^{re} in Eq. (40), we see contribution from F_Θ^{re} only. This is owing to the fact that if the initial input state of modes 3 and 4 is vacuum, mode 3 will remain being vacuum, making the generated hybrid state have no overlap with the ideal one $|\Psi\rangle_{13}$ in Eq. (5), of which mode 3 is a definite one-photon state. In other words, we have $F_0^{\text{re}} = 0$, explaining disappearance of the contribution due to F_0^{re} in the second equality of Eq. (40).

Some essential details for numerical calculations of the total realistic success probability P_T^{re} and the realistic fidelity F^{re} are given in Appendix A. In Fig. 4, we plot P_T^{re} (solid line) and F^{re} (dashed line) versus the type-II SPDC strength λ for two cases: (a) the squeezed vacuum as the approximate input cat state for mode 1 and (b) the squeezed single photon as the approximate input cat state for mode 1. Generally speaking, under consideration of the realistic inputs both P_T^{re} and F^{re} are reduced compared to the ideal case with the genuine input states. In particular, the total success probability P_T^{re} in both panels is of order 10^{-4}, which is three orders of magnitude lower than that in the ideal case (which is of order 10^{-1} as in Fig. 2). The fidelity F^{re} in both panels is less than one; for example, at $\lambda = 4\times10^{-2}$ one has $F^{\text{re}} \approx 0.25$ in panel (a) and $F^{\text{re}} \approx 0.94$ in panel (b). Comparing panels (a) and (b) at higher values of λ we see a clear outperformance of the squeezed single photon over the squeezed vacuum in terms of the total success probability and especially the fidelity. Discretely, at $\lambda = 8\times10^{-2}$ in panel (a) $P_T^{\text{re}} \approx 3.3\times10^{-4}$ and $F^{\text{re}} \approx 0.57$, while in

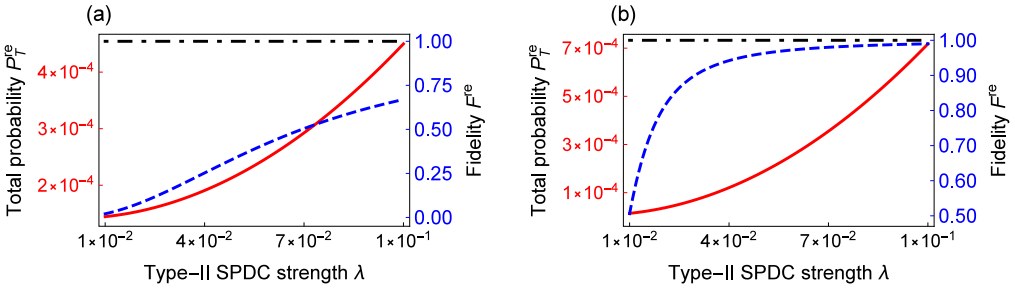

Fig. 4. (Color online) Total success probability P_T^{re} (solid line) and fidelity F^{re} (dashed line) in dependence on the type-II SPDC strength λ when using (a) the squeezed vacuum in Eq. (34) with $s = -0.43358$ as an approximation to an even cat state of amplitude 0.7 and (b) the squeezed single photon in Eq. (35) with $s = 0.16056$ as an approximation to an odd cat state of amplitude 0.7. In both panels, the dot-dashed line represents the unit fidelity (i.e., when the input states are perfect) and the reflectivity r is chosen to be 0.1.

panel (b) $P_T^{re} \approx 4.6 \times 10^{-4}$ and $F^{re} \approx 0.98$. Such superiority of the squeezed single photon is mainly thanks to its strong suppression in $P_{T,0}^{re}$. Numerically, we find $P_{T,0}^{re} \approx 1.4 \times 10^{-4}$, $P_{T,\Theta}^{re} \approx 3.1 \times 10^{-2}$, and $F_\Theta^{re} \approx 0.972$ for the case of the squeezed vacuum in panel (a) and $P_{T,0}^{re} \approx 6.9 \times 10^{-6}$, $P_{T,\Theta}^{re} \approx 7.1 \times 10^{-2}$, and $F_\Theta^{re} \approx 0.999$ for the case of the squeezed single photon in panel (b). By this, for large λ (say, $\lambda \geq 7 \times 10^{-2}$) the prefactor $\lambda^2 P_{T,\Theta}^{re}/P_T^{re}$ in Eq. (40) for the case of the squeezed vacuum varies from 0.52 to 0.69, but for the case of the squeezed single photon it is very close to 1 ranging from 0.98 to 0.99, which in turn renders the average fidelity F^{re} roughly equal to F_Θ^{re}.

3.3. Imperfections in balanced beam splitters

The setup in Fig. 1 requires using two BBSs (i.e., BBS1 and BBS2) as well as several PBSs and one HWP. We assume that the PBSs and the HWP are perfect but consider the circumstance when the two BBSs could be slightly unbalanced. To this end, we introduce small imperfection parameters ϵ_k with $k = 1, 2$ defined via the reflectivity and the transmissivity of the imperfect BBS1 and BBS2 as

$$\epsilon_k = 1/2 - r_k = t_k - 1/2. \tag{41}$$

Reasonably, we assume $|\epsilon_k| \ll 1$ to ensure a slight unbalance of the BBSs.

Because of the asymmetry of the two imperfect BBSs, the outcomes of the four measurements characterized by the operators $\{\Pi_j; j = 1, 2, 3, 4\}$ defined respectively in Eqs. (20)–(23) will herald successful generation of the hybrid entangled state with different success probabilities P_j^{im} and fidelities F_j^{im}. Analytical expressions for P_j^{im} and F_j^{im} are derived in Appendix B and in this subsection we highlight essential results only. Generally, P_j^{im} and F_j^{im} depend not only on ϵ_1 and ϵ_2 but also on j. For example, regarding the measurement Π_1 we find that

$$P_1^{im} = N^2(\beta)\left[(r_2^2 + t_2^2) r\beta^2 e^{-2r\beta^2} + (r_2^2 - t_2^2)\gamma_1\gamma_2 e^{-2\beta^2}\right] \tag{42}$$

and

$$F_1^{im} = \frac{N^2(\beta)e^{-2r\beta^2}}{4P_1^{im}}\left[\gamma_2 f_0(\delta_1)(r_2\langle\delta|\delta_2\rangle - t_2\langle-\delta|\delta_2\rangle) + \gamma_1 f_0(\delta_2)\langle\delta|\delta_1\rangle\right]^2, \tag{43}$$

where δ is defined below Eq. (12) and $f_n(x)$ is defined above Eq. (13), while γ_1, γ_2, δ_1, and δ_2 are some constants dependent on β, r, t and $\epsilon_{1,2}$ (see the corresponding formulae in Appendix B). As for $P_{2,3,4}^{im}$ and $F_{2,3,4}^{im}$, their expressions are given explicitly in Appendix B, which are j-dependent. However, we find out that the total success probability P_T^{im} turns out to be the same as in the ideal case. That is,

$$P_T^{im} = \sum_{j=1}^{4} P_j^{im} = P_T, \tag{44}$$

where $P_T = 4P$ with P given in Eq. (24). This shows that the total success probability of our generation scheme is insensitive to small BBS imperfections. For analysis of the fidelity, we define its average as

$$\bar{F}^{im} = \frac{\sum_{j=1}^{4} P_j^{im} F_j^{im}}{\sum_{j=1}^{4} P_j^{im}}, \tag{45}$$

which depends on both ϵ_1 and ϵ_2. In Fig. 5 we plot $\bar{F}^{im}$ as a function of ϵ_1 and ϵ_2. As seen clearly from the plot, $\bar{F}^{im}$ remains very high (i.e., $\bar{F}^{im} \geq 0.980$) for $|\epsilon_{1,2}| \leq 0.08$. The value of $\bar{F}^{im}$ is approaching 1 when $\epsilon_{1,2}$ are tending to zero. More concretely, $\bar{F}^{im} \geq 0.999$ for $|\epsilon_{1,2}| \leq 0.02$.

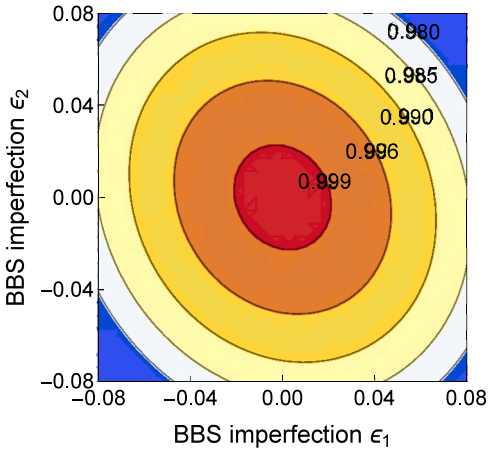

Fig. 5. (Color online) Average fidelity $\bar{F}^{\rm im}$ defined in Eq. (45) in variation with respect to the BBS imperfection parameters ϵ_1 and ϵ_2. Here to generate the plot β and r are chosen similarly to those in Fig. 3.

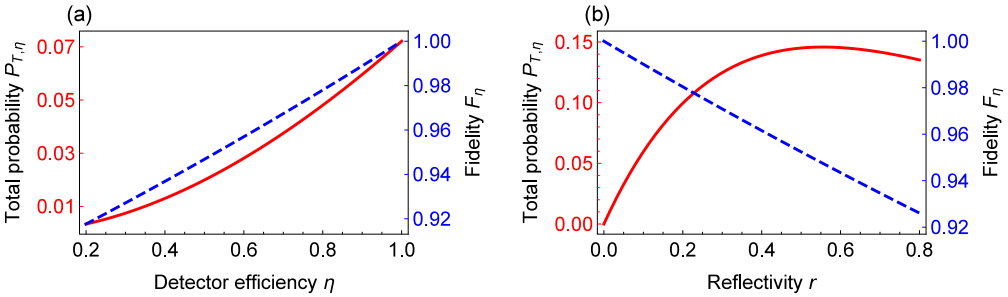

Fig. 6. (Color online) Total probability $P_{T,\eta}$ (solid line) given in Eq. (48) and fidelity F_η (dashed line) given in Eq. (49) in dependence on (a) the detector efficiency η and (b) the reflectivity r. In panel (a) the reflectivity r is 0.1, while in panel (b) the photodetector efficiency η is 0.9. In both panels, we assume perfect input states of which the input even cat state has an amplitude $\beta = 1$.

3.4. Inefficient photodetectors

A crucial requirement in our scheme is that the photodetectors are able to resolve photon numbers. However, practical photodetectors are often inefficient operating with some errors. We thus take into account such imperfect photodetectors whose figure of merit is characterized by the efficiency $\eta \in [0, 1]$. Mathematically, a detection of n photons with efficiency η is modeled by a positive operator-valued measurement (POVM) [44]

$$E^{(n)}_{\eta,a} = \sum_{k=0}^{\infty} C^k_{n+k} \eta^n (1-\eta)^k |n+k\rangle_a\langle n+k|, \tag{46}$$

where a denotes the mode whose photon number is detected. For $\eta = 1$, $E^{(n)}_{\eta=1,a} \equiv |n\rangle_a\langle n|$, representing a perfect projective measurement. For $\eta \to 0$ and $n \neq 0$, $E^{(n)}_{\eta\to 0,a} \to 0$, implying no information about the measured state can be obtained. The perfect measurement Π_1 in Eq. (20) is then replaced by an imperfect one $\Pi_{1,\eta}$ which is of the form

$$\Pi_{1,\eta} = E^{(0)}_{\eta,2} \otimes E^{(1)}_{\eta,2'} \otimes E^{(1)}_{\eta,4} \otimes E^{(0)}_{\eta,4'}, \tag{47}$$

and similar replacements are made for Π_2, Π_3, and Π_4.

For the input states of the forms given in Eqs. (7)–(9) the total success probability $P_{T,\eta}$ and the fidelity F_η in the presence of inefficient photodetectors are derived as

$$P_{T,\eta} = \frac{r\beta^2\eta^2 e^{-2r\beta^2\eta}}{1 + e^{-2\beta^2}}, \tag{48}$$

$$F_\eta = \frac{1 + e^{-2r\beta^2(1-\eta)}}{2}. \tag{49}$$

In Fig. 6 we plot $P_{T,\eta}$ (solid line) and F_η (dashed line) as a function of (a) the detector efficiency η and (b) the reflectivity r. For panel (a), variations of the total success probability $P_{T,\eta}$ and the fidelity F_η share the same pattern, that is, monotonic increase

Table 1
Comparisons of types of hybrid entangled state to be generated, total success probabilities, and resource consumptions between our scheme and others.

	Our scheme	The schemes in Refs. [41,42]
Type of hybrid entanglement	$\frac{1}{\sqrt{2}}(\|\alpha_H\rangle\|H\rangle + \|-\alpha_V\rangle\|V\rangle)$	$\frac{1}{\sqrt{2}}(\|\alpha\rangle\|H\rangle + \|-\alpha\rangle\|V\rangle)$
Total success probability	$4P$ with P given in Eq. (24)	$2P$
Resource consumption	Passive devices and photon-number-resolving detectors	Active displacement, passive devices, and photon-number-resolving detectors

with the efficiency η. This is as expected, since the better the detectors are the better the scheme performance is. By contrast, in panel (b) we observe a tradeoff between $P_{T,\eta}$ and F_η in terms of the reflectivity r. Concretely, an increase in r results in a higher $P_{T,\eta}$ with a sacrifice of a lower F_η. For example, with $r = \{0.1, 0.2, 0.3, \ldots\}$ we have $P_{T,\eta} = \{0.0596, 0.0996, 0.1247, \ldots\}$ and $F_\eta = \{0.990, 0.980, 0.971, \ldots\}$. This can be qualitatively explained as follows. Increasing r leads to improvements in both the single-photon population, i.e., the function $f_1^2(\gamma)$ with $\gamma = \beta\sqrt{2r}$ in Eq. (24), and the n-photon populations, $f_n^2(\gamma)$ $(n > 1)$, in mode 2 of the state $|\Xi\rangle_{12}$ in Eq. (12). The first improvement directly links to an increase in the total success probability (see Eq. (24)). As for the second one, it deserves noting that the detectors are now imperfect, so that the collapsed state of modes 1 and 3 after a measurement, say, $\Pi_{1,\eta}$, contains not only the desired hybrid entangled state in Eq. (17) but also irrelevant terms hidden in "OT" of Eq. (16) whose weights increase with $f_n^2(\gamma)$. The second improvement in $f_n^2(\gamma)$ thus enhances the populations of these unwanted terms in the generated state which have no overlap with the target one and, as a result, degrades the fidelity. Furthermore, we note from Eqs. (48) and (49) that $\lim_{r\to 0} P_{T,\eta} = 0$ and $\lim_{r\to 0} F_\eta = 1$, implying that for any given efficiency η an arbitrarily high fidelity can be achieved by decreasing the reflectivity r yet with a price of an arbitrarily low success probability.

4. Discussion and conclusion

For a glance at the differences in our generation scheme in comparison with others we first provide the main concerned features in Table 1 and then go into detailed discussions.

Unlike the scheme in Ref. [41], where the input mode of the first party is an unpolarized Schrodinger cat state and thus his/her two-mode entangled state is also unpolarized, in our scheme the input mode of the first party is a polarized Schrodinger cat state (see Eq. (7)) and thus his/her two-mode entangled state is also polarized (see Eq. (12)). The advantage of using polarized modes is that now a mode is characterized at the same time by two DoFs: path DoF and polarization DoF. Since a photon in the two-particle entangled polarization state in Eq. (9) also has both path and polarization DoFs and after the second BBS (i.e., BBS2) in Fig. 1 all the path and polarization information are erased, we have four successful events in our scheme rather than only two in the schemes of Refs. [41,42]. This explains why our total success probability doubles in comparison to that in Refs. [41,42].

Another positive point of our scheme is that we do not use displacement operation as in Refs. [41,42]. Since in practice displacement operation can only be implemented approximately by means of a highly transmissive BS plus a strong local coherent beam [48], avoiding such operation as in our scheme allows achieving exact unit fidelity and relaxes resource consumption.

Analyses of decoherence effect on the input states and imperfection of the BBSs show that our scheme remains resilient against small perturbations. Particularly, reasonable success probability (> 0.1) and high fidelity (> 0.9) can be retained, provided that the decoherence strength is weak enough and the BBSs' imperfections are small enough. The former condition can be satisfied by properly designing an experimental setup that minimizes the interaction time of the input states with their surrounding environments, whereas the latter condition by carefully engineering optical devices.

To obtain the desired hybrid entanglement $|\Psi\rangle_{13} = \left(|\alpha_H\rangle_1|H\rangle_3 + |-\alpha_V\rangle_1|V\rangle_3\right)/\sqrt{2}$ with a reasonably large amplitude α, two requirements should be simultaneously met: (i) the amplitude β of the input state $|\Gamma\rangle_1 = N(\beta)\left(|\beta_H\rangle + |-\beta_H\rangle\right)_1$ should be large enough and (ii) the reflectivity r of the general BS (i.e., BS(r) in part 2 of the setup in Fig. 1) should be low enough. Schrodinger even and odd kitten states (i.e., cat states with small amplitudes) can be approximated by the squeezed vacuum and the squeezed single photon with very high fidelities [25,40,58–60] and it is also possible to feed such a kitten to grow up to a cat [64]. Hence the requirement (i) could in principle be met. As for the requirement (ii), it stems from the relation (18) and is straightforwardly satisfied, since a BS with arbitrarily low reflectivity (high transmissivity) can be engineered with current technologies. In addition, it is significant to take into account the realistic entangled polarization photon pair $|\Theta\rangle_{34}$, which is typically mixed with a strong vacuum. Such vacuum mixing in general reduces the scheme success probability and the fidelity. One way to deal with this issue is to use a heralded entangled photon source [65–67], which however could complicate the whole experimental setup. A simpler solution is to employ an (approximate) odd cat state as the input for mode 1, by which a high fidelity can still be achieved (see Section 3.2).

Another practical issue of great concern is that failure occurs whenever a detector registers multiple photons that is caused by the terms contained in "OT" of Eq. (16). To correctly discriminate between success and failure, photon-number-resolving detectors are necessitated. On the one hand, photon-number-resolving detectors with efficiency as high as 95% have been demonstrated [68] and employed in various experiments [69–71]. On the other hand, as pointed out in Section 3.4, even with photodetectors of low efficiency, reduction of the reflectivity of the general BS used in our scheme would yield a rather high fidelity but at the cost

of a quite low success probability. Additionally, propagation of modes along different optical paths may cause bad effects if the differences in modal accumulated phases become big. In that case the relative phase needs to be kept constant in order to achieve the generated state with high fidelity. One approach to do so is by means of the phase-locking technique described in Ref. [40] which employs ancillary seed weak beams and photodiodes.

To conclude, we have presented a new scheme to prepare an entangled state between a polarized coherent state and a polarized photon. The proposed scheme is of interest from both theoretical and experimental points of view. It is interestingly associated with a new, promising qubit encoding in Eq. (6). As a possible application, our generated entangled state can serve as a quantum channel for two parties, Alice and Bob, to do hybrid teleportation: either Alice teleports an unknown DV qubit $c|H\rangle + d|V\rangle$ to Bob who receives a CV qubit $\mathcal{N}(c|\alpha_H\rangle + d|-\alpha_V\rangle)$ or, in the opposite direction, Bob teleports an unknown CV qubit $\mathcal{N}(c|\alpha_H\rangle + d|-\alpha_V\rangle)$ to Alice who receives a DV qubit $c|H\rangle + d|V\rangle$. Of great benefit is the fact that all of the in-line operations in our scheme are manipulated only by means of commonly available passive optical elements such as BSs, BBSs, HWPs, and PBSs once the necessary inputs including a cat state, a coherent state, and a pair of entangled polarized photons are supplied off-line. Besides achieving a doubled total success probability compared with that in Refs. [41,42], our scheme is also economical because no resource-consuming displacement operators are needed. Moreover, detailed analyses have shown that our scheme is robust against small decoherence effect and device imperfections and its relevant technical requirements can be met within current technology making it experimentally feasible.

Declaration of competing interest

The authors declare that they have no known competing financial interests or personal relationships that could have appeared to influence the work reported in this paper.

Acknowledgments

We thank Kaumudibikash Goswami, Jihun Cha, Warit Asavanant, and Mikkel V. Larsen for useful discussions and Rohit Navarathna for the help with cluster computation. In this work D.T.L is supported by the Australian Research Council Centre of Excellence for Engineered Quantum Systems (EQUS, CE170100009), while C.T.B. and N.B.A. are supported by the National Foundation for Science and Technology Development (NAFOSTED VN) under Project No. 103.01–2019.313.

Appendix A. Realistic resources for the input states

Using the squeezed vacuum state $|\mathrm{sv}\rangle$ in Eq. (34) as the approximate input even cat state for mode 1 and the entangled polarization photon pair state $|\Theta\rangle_{34}$ in Eq. (9) as the input for modes 3 and 4 and noting the application of a general BS on Fock states in Eq. (14), the total state $|\Sigma\rangle$ in Eq. (13) of modes $1, 2, 3$, and 4 which already passed through part 1 and the general BS in part 2 of the setup in Fig. 1 is altered to be

$$|\Sigma^{\mathrm{ap}}\rangle = \sum_{n,m=0}^{\infty} \sum_{p=0}^{\bar{n}} \sum_{q=0}^{m} \sum_{p'=0}^{\bar{n}-p+q} \sum_{q'=0}^{m-q+p} F^{n,m}_{p,q,p',q'}(s,\beta,r,t)\, |(\bar{n}-p+q-p')_H, (m-q+p-q')_V\rangle_1 |p'_H, q'_V\rangle_2 \otimes \frac{1}{\sqrt{2}}\left(|H\rangle_3|V\rangle_4 + |V\rangle_3|H\rangle_4\right), \tag{A.1}$$

where $\bar{n} = 2n$, and

$$F^{n,m}_{p,q,p',q'}(s,\beta,r,t) = c_n(s) f_m(\beta) B^{\bar{n},m}_{p,q}(\tfrac{1}{2},\tfrac{1}{2}) B^{\bar{n}-p+q,0}_{p',0}(r,t) B^{m-q+p,0}_{q',0}(r,t), \tag{A.2}$$

$$c_n(s) = \frac{(-\tanh s)^n}{(\cosh s)^{1/2}} \frac{\sqrt{(2n)!}}{2^n n!}, \tag{A.3}$$

with $c_n(s)$ the coefficient of the squeezed vacuum state $|\mathrm{sv}\rangle$ in Eq. (34) and $f_n(x)$ and $B^{j,k}_{p,q}(r,t)$ defined by Eqs. (13) and (15), respectively. Modes 2 and 4 then interfere at the BBS2 and afterwards enter two PBSs (see part 2 of the setup in Fig. 1), yielding the output state as

$$\begin{aligned}
|\Sigma^{\mathrm{ap}\prime}\rangle = {} & \frac{1}{\sqrt{2}} \sum_{n,m=0}^{\infty} \sum_{p=0}^{\bar{n}} \sum_{q=0}^{m} \sum_{p'=0}^{\bar{n}-p+q} \sum_{q'=0}^{m-q+p} \sum_{k=0}^{p'} \sum_{k'=0}^{q'} \sum_{l'=0}^{1} F^{n,m}_{p,q,p',q'}(s,\beta,r,t) \\
& \times B^{p',0}_{k,0}(\tfrac{1}{2},\tfrac{1}{2}) B^{q',1}_{k',l'}(\tfrac{1}{2},\tfrac{1}{2}) |(\bar{n}-p+q-p')_H, (m-q+p-q')_V\rangle_1 |1_H\rangle_3 |(p'-k)_H\rangle_2 |k_H\rangle_4 |(q'-k'+l')_V\rangle_{2'} |(1-l'+k')_V\rangle_{4'} \\
& + \frac{1}{\sqrt{2}} \sum_{n,m=0}^{\infty} \sum_{p=0}^{\bar{n}} \sum_{q=0}^{m} \sum_{p'=0}^{\bar{n}-p+q} \sum_{q'=0}^{m-q+p} \sum_{k=0}^{p'} \sum_{l=0}^{1} \sum_{k'=0}^{q'} F^{n,m}_{p,q,p',q'}(s,\beta,r,t) \\
& \times B^{p',1}_{k,l}(\tfrac{1}{2},\tfrac{1}{2}) B^{q',0}_{k',0}(\tfrac{1}{2},\tfrac{1}{2}) |(\bar{n}-p+q-p')_H, (m-q+p-q')_V\rangle_1 |1_V\rangle_3 |(p'-k+l)_H\rangle_2 |(1-l+k)_H\rangle_4 |(q'-k')_V\rangle_{2'} |k'_V\rangle_{4'}.
\end{aligned} \tag{A.4}$$

After the measurement Π_1 defined in Eq. (20), modes 1 and 3 in the state $|\Sigma^{\mathrm{ap}\prime}\rangle$ are projected onto

$$\rho_1^{(13)} = \frac{\mathrm{Tr}_{22'44'}\left(\Pi_1 |\Sigma^{\mathrm{ap}\prime}\rangle\langle\Sigma^{\mathrm{ap}\prime}|\right)}{P^{\mathrm{re}}_{1,\Theta}}, \tag{A.5}$$

where

$$P^{\rm re}_{1,\Theta} = \langle \Sigma^{\rm ap'} | \Pi_1 | \Sigma^{\rm ap'} \rangle \tag{A.6}$$

is the heralding probability. This yields the fidelity between the prepared state $\rho_1^{(13)}$ and the genuine hybrid entangled state $|\Psi\rangle_{13}$ as

$$F^{\rm re}_{1,\Theta} = {}_{13}\langle \Psi | \rho_1^{(13)} | \Psi \rangle_{13}. \tag{A.7}$$

Similarly, we can calculate the probabilities $P^{\rm re}_{j,\Theta}$ and the fidelities $F^{\rm re}_{j,\Theta}$ for the other three measurements $\Pi_{j=2,3,4}$ defined in Eqs. (21)–(23) . The above procedure is repeated when replacing the entangled polarization pair $(|H\rangle|V\rangle + |V\rangle|H\rangle)/\sqrt{2}$ of modes 3 and 4 in Eq. (A.1) with vacuum to obtain $P^{\rm re}_{j,0}$ and/or replacing the squeezed vacuum state $|{\rm sv}\rangle$ as the input state for mode 1 with the squeezed single photon state $|{\rm ss}\rangle$ in Eq. (35). We also would like to note that in performing our numerical calculations the cutoff upper limit for the indexes n and m in Eq. (A.4) is chosen to be 7 [41].

Appendix B. Balanced beam splitter imperfections

For consideration of BBS imperfections in Section 3.3, we respectively replace the two perfect BBSs in the setup of Fig. 1 (i.e., BBS1 and BBS2) by the imperfect ones BS(r_1, t_1) and BS(r_2, t_2), with r_k and t_k being different from 1/2 by small imperfection parameters ϵ_k as defined in Eq. (41). We then recalculate Section 2 with these general BSs for the measurement Π_1 defined in Eq. (20) and find $P^{\rm im}_1$ and $F^{\rm im}_1$ as in Eqs. (42) and (43) with

$$\gamma_1 = \beta(\sqrt{t_1} + \sqrt{r_1})\sqrt{r}, \tag{B.1a}$$

$$\gamma_2 = \beta(\sqrt{r_1} - \sqrt{t_1})\sqrt{r}, \tag{B.1b}$$

$$\delta_1 = \beta(\sqrt{t_1} + \sqrt{r_1})\sqrt{t}, \tag{B.1c}$$

$$\delta_2 = \beta(\sqrt{r_1} - \sqrt{r_1})\sqrt{t}. \tag{B.1d}$$

Analogously for the other three measurements $\{\Pi_j; j = 2,3,4\}$ defined in Eqs. (21)–(23), we find correspondingly the success probabilities $P^{\rm im}_j$ and the fidelities $F^{\rm im}_j$ as the following

$$P^{\rm im}_2 = N^2(\beta)\left[(r_2^2+t_2^2)r\beta^2 e^{-2r\beta^2} - (r_2^2-t_2^2)\gamma_1\gamma_2 e^{-2\beta^2}\right], \tag{B.2}$$

$$F^{\rm im}_2 = \frac{N^2(\beta)e^{-2r\beta^2}}{4P^{\rm im}_2}\left[\gamma_2 f_0(\delta_1)(t_2\langle\delta|\delta_2\rangle - r_2\langle -\delta|\delta_2\rangle) + \gamma_1 f_0(\delta_2)\langle\delta|\delta_1\rangle\right]^2, \tag{B.3}$$

$$P^{\rm im}_3 = P^{\rm im}_4 = 4r_2t_2P, \tag{B.4}$$

$$F^{\rm im}_3 = F^{\rm im}_4 = \frac{N^2(\beta)}{4P^{\rm im}_3}(A_3 + B_3)^2, \tag{B.5}$$

$$A_3 = 2f_0(\delta_2)\sqrt{r_2t_2}\gamma_1 e^{-r\beta^2}\langle\delta|\delta_1\rangle, \tag{B.6}$$

$$B_3 = f_0(\delta_1)\sqrt{r_2t_2}\gamma_2 e^{-r\beta^2}(\langle\delta|\delta_2\rangle - \langle -\delta|\delta_2\rangle), \tag{B.7}$$

where $f_n(x)$ is the coherent-state coefficient defined above Eq. (13) and P is given in Eq. (24). Without difficulty one can check that

$$\sum_j^4 P^{\rm im}_j = 4P \equiv P_T, \tag{B.8}$$

where P_T is the total success probability in the ideal case.

References

[1] G. Kurizki, P. Bertet, Y. Kubo, K. Mølmer, D. Petrosyan, P. Rabl, J. Schmiedmayer, Quantum technologies with hybrid systems, Proc. Natl. Acad. Sci. USA 112 (13) (2015) 3866–3873, http://dx.doi.org/10.1073/pnas.1419326112.

[2] U.L. Andersen, J.S. Neergaard-Nielsen, P. van Loock, A. Furusawa, Hybrid discrete- and continuous-variable quantum information, Nat. Phys. 11 (9) (2015) 713–719, http://dx.doi.org/10.1038/nphys3410.

[3] A.W. Elshaari, W. Pernice, K. Srinivasan, O. Benson, V. Zwiller, Hybrid integrated quantum photonic circuits, Nat. Photonics (2020) http://dx.doi.org/10.1038/s41566-020-0609-x.

[4] G. Guccione, T. Darras, H. Le Jeannic, V.B. Verma, S.W. Nam, A. Cavaillès, J. Laurat, Connecting heterogeneous quantum networks by hybrid entanglement swapping, Sci. Adv. 6 (22) (2020) http://dx.doi.org/10.1126/sciadv.aba4508.

[5] F. De Martini, F. Sciarrino, C. Vitelli, Entanglement test on a microscopic-macroscopic system, Phys. Rev. Lett. 100 (2008) 253601, http://dx.doi.org/10.1103/PhysRevLett.100.253601.

[6] P. Sekatski, N. Sangouard, M. Stobińska, F. Bussières, M. Afzelius, N. Gisin, Proposal for exploring macroscopic entanglement with a single photon and coherent states, Phys. Rev. A 86 (2012) 060301, http://dx.doi.org/10.1103/PhysRevA.86.060301.

[7] N. Bruno, A. Martin, P. Sekatski, N. Sangouard, R.T. Thew, N. Gisin, Displacement of entanglement back and forth between the micro and macro domains, Nat. Phys. 9 (9) (2013) 545–548, http://dx.doi.org/10.1038/nphys2681.

[8] A.I. Lvovsky, R. Ghobadi, A. Chandra, A.S. Prasad, C. Simon, Observation of micro–macro entanglement of light, Nat. Phys. 9 (9) (2013) 541–544, http://dx.doi.org/10.1038/nphys2682.

[9] U.L. Andersen, J.S. Neergaard-Nielsen, Heralded generation of a micro-macro entangled state, Phys. Rev. A 88 (2013) 022337, http://dx.doi.org/10.1103/PhysRevA.88.022337.

[10] R. Ghobadi, A. Lvovsky, C. Simon, Creating and detecting micro-macro photon-number entanglement by amplifying and deamplifying a single-photon entangled state, Phys. Rev. Lett. 110 (2013) 170406, http://dx.doi.org/10.1103/PhysRevLett.110.170406.

[11] R. Ghobadi, S. Kumar, B. Pepper, D. Bouwmeester, A.I. Lvovsky, C. Simon, Optomechanical micro-macro entanglement, Phys. Rev. Lett. 112 (2014) 080503, http://dx.doi.org/10.1103/PhysRevLett.112.080503.

[12] A. Tiranov, J. Lavoie, P.C. Strassmann, N. Sangouard, M. Afzelius, F. Bussières, N. Gisin, Demonstration of light-matter micro-macro quantum correlations, Phys. Rev. Lett. 116 (2016) 190502, http://dx.doi.org/10.1103/PhysRevLett.116.190502.

[13] E. Schrödinger, Die gegenwärtige Situation in der Quantenmechanik, Naturwissenschaften 23 (48) (1935) 807–812, http://dx.doi.org/10.1007/BF01491891.

[14] P. van Loock, Optical hybrid approaches to quantum information, Laser Photonics Rev. 5 (2) (2011) 167–200, http://dx.doi.org/10.1002/lpor.201000005.

[15] K. Park, H. Jeong, Entangled coherent states versus entangled photon pairs for practical quantum-information processing, Phys. Rev. A 82 (2010) 062325, http://dx.doi.org/10.1103/PhysRevA.82.062325.

[16] S.L. Braunstein, P. van Loock, Quantum information with continuous variables, Rev. Modern Phys. 77 (2005) 513–577, http://dx.doi.org/10.1103/RevModPhys.77.513.

[17] S.L. Braunstein, A.K. Pati, Quantum Information with Continuous Variables, Springer, Dordrecht, 2010.

[18] K. Huang, H.L. Jeannic, O. Morin, T. Darras, G. Guccione, A. Cavaillès, J. Laurat, Engineering optical hybrid entanglement between discrete- and continuous-variable states, New J. Phys. 21 (8) (2019) 083033, http://dx.doi.org/10.1088/1367-2630/ab34e7.

[19] S. Takeda, T. Mizuta, M. Fuwa, P. van Loock, A. Furusawa, Deterministic quantum teleportation of photonic quantum bits by a hybrid technique, Nature 500 (7462) (2013) 315–318, http://dx.doi.org/10.1038/nature12366.

[20] S. Takeda, M. Fuwa, P. van Loock, A. Furusawa, Entanglement swapping between discrete and continuous variables, Phys. Rev. Lett. 114 (2015) 100501, http://dx.doi.org/10.1103/PhysRevLett.114.100501.

[21] K. Park, S.-W. Lee, H. Jeong, Quantum teleportation between particlelike and fieldlike qubits using hybrid entanglement under decoherence effects, Phys. Rev. A 86 (2012) 062301, http://dx.doi.org/10.1103/PhysRevA.86.062301.

[22] Y.-B. Sheng, L. Zhou, G.-L. Long, Hybrid entanglement purification for quantum repeaters, Phys. Rev. A 88 (2013) 022302, http://dx.doi.org/10.1103/PhysRevA.88.022302.

[23] A.E. Ulanov, D. Sychev, A.A. Pushkina, I.A. Fedorov, A.I. Lvovsky, Quantum teleportation between discrete and continuous encodings of an optical qubit, Phys. Rev. Lett. 118 (2017) 160501, http://dx.doi.org/10.1103/PhysRevLett.118.160501.

[24] H.L. Jeannic, A. Cavaillès, J. Raskop, K. Huang, J. Laurat, Remote preparation of continuous-variable qubits using loss-tolerant hybrid entanglement of light, Optica 5 (8) (2018) 1012–1015, http://dx.doi.org/10.1364/OPTICA.5.001012.

[25] D.V. Sychev, A.E. Ulanov, E.S. Tiunov, A.A. Pushkina, A. Kuzhamuratov, V. Novikov, A.I. Lvovsky, Entanglement and teleportation between polarization and wave-like encodings of an optical qubit, Nature Commun. 9 (1) (2018) 3672, http://dx.doi.org/10.1038/s41467-018-06055-x.

[26] H. Jeong, Using weak nonlinearity under decoherence for macroscopic entanglement generation and quantum computation, Phys. Rev. A 72 (2005) 034305, http://dx.doi.org/10.1103/PhysRevA.72.034305.

[27] T.P. Spiller, K. Nemoto, S.L. Braunstein, W.J. Munro, P. van Loock, G.J. Milburn, Quantum computation by communication, New J. Phys. 8 (2) (2006) 30, http://dx.doi.org/10.1088/1367-2630/8/2/030.

[28] P. van Loock, W.J. Munro, K. Nemoto, T.P. Spiller, T.D. Ladd, S.L. Braunstein, G.J. Milburn, Hybrid quantum computation in quantum optics, Phys. Rev. A 78 (2008) 022303, http://dx.doi.org/10.1103/PhysRevA.78.022303.

[29] S.-W. Lee, H. Jeong, Near-deterministic quantum teleportation and resource-efficient quantum computation using linear optics and hybrid qubits, Phys. Rev. A 87 (2013) 022326, http://dx.doi.org/10.1103/PhysRevA.87.022326.

[30] J. Joo, W.J. Munro, T.P. Spiller, Quantum metrology with entangled coherent states, Phys. Rev. Lett. 107 (2011) 083601, http://dx.doi.org/10.1103/PhysRevLett.107.083601.

[31] H. Kwon, H. Jeong, Violation of the Bell–Clauser-Horne-Shimony-Holt inequality using imperfect photodetectors with optical hybrid states, Phys. Rev. A 88 (2013) 052127, http://dx.doi.org/10.1103/PhysRevA.88.052127.

[32] M. Stobińska, F. Töppel, P. Sekatski, A. Buraczewski, Towards loophole-free Bell inequality test with preselected unsymmetrical singlet states of light, Phys. Rev. A 89 (2014) 022119, http://dx.doi.org/10.1103/PhysRevA.89.022119.

[33] A. Cavaillès, H. Le Jeannic, J. Raskop, G. Guccione, D. Markham, E. Diamanti, M.D. Shaw, V.B. Verma, S.W. Nam, J. Laurat, Demonstration of Einstein–Podolsky–Rosen steering using hybrid continuous- and discrete-variable entanglement of light, Phys. Rev. Lett. 121 (2018) 170403, http://dx.doi.org/10.1103/PhysRevLett.121.170403.

[34] N.B. An, L.T. Dat, J. Kim, Nonstandard protocols for joint remote preparation of a general quantum state and hybrid entanglement of any dimension, Phys. Rev. A 98 (2018) 042329, http://dx.doi.org/10.1103/PhysRevA.98.042329.

[35] Z.-X. Man, Y.-J. Xia, N.B. An, Simultaneous observation of particle and wave behaviors of entangled photons, Sci. Rep. 7 (1) (2017) 42539, http://dx.doi.org/10.1038/srep42539.

[36] A.S. Rab, E. Polino, Z.-X. Man, N. Ba An, Y.-J. Xia, N. Spagnolo, R. Lo Franco, F. Sciarrino, Entanglement of photons in their dual wave-particle nature, Nature Commun. 8 (1) (2017) 915, http://dx.doi.org/10.1038/s41467-017-01058-6.

[37] L.S. Costanzo, A. Zavatta, S. Grandi, M. Bellini, H. Jeong, M. Kang, S.-W. Lee, T.C. Ralph, Experimental hybrid entanglement between quantum and classical states of light, Int. J. Quantum Inf. 12 (07n08) (2014) 1560015, http://dx.doi.org/10.1142/S0219749915600151.

[38] H. Jeong, A. Zavatta, M. Kang, S.-W. Lee, L.S. Costanzo, S. Grandi, T.C. Ralph, M. Bellini, Generation of hybrid entanglement of light, Nat. Photonics 8 (7) (2014) 564–569, http://dx.doi.org/10.1038/nphoton.2014.136.

[39] E. Agudelo, J. Sperling, L.S. Costanzo, M. Bellini, A. Zavatta, W. Vogel, Conditional hybrid nonclassicality, Phys. Rev. Lett. 119 (2017) 120403, http://dx.doi.org/10.1103/PhysRevLett.119.120403.

[40] O. Morin, K. Huang, J. Liu, H. Le Jeannic, C. Fabre, J. Laurat, Remote creation of hybrid entanglement between particle-like and wave-like optical qubits, Nat. Photonics 8 (7) (2014) 570–574, http://dx.doi.org/10.1038/nphoton.2014.137.

[41] H. Kwon, H. Jeong, Generation of hybrid entanglement between a single-photon polarization qubit and a coherent state, Phys. Rev. A 91 (2015) 012340, http://dx.doi.org/10.1103/PhysRevA.91.012340.

[42] S. Li, H. Yan, Y. He, H. Wang, Experimentally feasible generation protocol for polarized hybrid entanglement, Phys. Rev. A 98 (2018) 022334, http://dx.doi.org/10.1103/PhysRevA.98.022334.

[43] P. Kok, W.J. Munro, K. Nemoto, T.C. Ralph, J.P. Dowling, G.J. Milburn, Linear optical quantum computing with photonic qubits, Rev. Modern Phys. 79 (2007) 135–174, http://dx.doi.org/10.1103/RevModPhys.79.135.

[44] P. Kok, B.W.L. Lovett, Introduction to Optical Quantum Information Processing, Cambridge University Press, Cambridge, 2010.

[45] M. Lobino, C. Kupchak, E. Figueroa, A.I. Lvovsky, Memory for light as a quantum process, Phys. Rev. Lett. 102 (2009) 203601, http://dx.doi.org/10.1103/PhysRevLett.102.203601.

[46] H. Jeong, S. Bae, S. Choi, Quantum teleportation between a single-rail single-photon qubit and a coherent-state qubit using hybrid entanglement under decoherence effects, Quantum Inf. Process. 15 (2) (2016) 913–927, http://dx.doi.org/10.1007/s11128-015-1191-x.
[47] H. Kim, S.-W. Lee, H. Jeong, Two different types of optical hybrid qubits for teleportation in a lossy environment, Quantum Inf. Process. 15 (11) (2016) 4729–4746, http://dx.doi.org/10.1007/s11128-016-1408-7.
[48] M.G. Paris, Displacement operator by beam splitter, Phys. Lett. A 217 (2) (1996) 78–80, http://dx.doi.org/10.1016/0375-9601(96)00339-8.
[49] S.-Y. Lee, C.-W. Lee, P. Kurzyński, D. Kaszlikowski, J. Kim, Duality in entanglement of macroscopic states of light, Phys. Rev. A 94 (2016) 022314, http://dx.doi.org/10.1103/PhysRevA.94.022314.
[50] H. Jeong, M.S. Kim, Efficient quantum computation using coherent states, Phys. Rev. A 65 (2002) 042305, http://dx.doi.org/10.1103/PhysRevA.65.042305.
[51] G.A. Barbosa, E. Corndorf, P. Kumar, H.P. Yuen, Secure communication using mesoscopic coherent states, Phys. Rev. Lett. 90 (2003) 227901, http://dx.doi.org/10.1103/PhysRevLett.90.227901.
[52] G.A. Barbosa, Fast and secure key distribution using mesoscopic coherent states of light, Phys. Rev. A 68 (2003) 052307, http://dx.doi.org/10.1103/PhysRevA.68.052307.
[53] W.-H. Kye, C.-M. Kim, M.S. Kim, Y.-J. Park, Quantum key distribution with blind polarization bases, Phys. Rev. Lett. 95 (2005) 040501, http://dx.doi.org/10.1103/PhysRevLett.95.040501.
[54] S. Lorenz, J. Rigas, M. Heid, U.L. Andersen, N. Lütkenhaus, G. Leuchs, Witnessing effective entanglement in a continuous variable prepare-and-measure setup and application to a quantum key distribution scheme using postselection, Phys. Rev. A 74 (2006) 042326, http://dx.doi.org/10.1103/PhysRevA.74.042326.
[55] H.F. Hofmann, T. Ono, High-photon-number path entanglement in the interference of spontaneously down-converted photon pairs with coherent laser light, Phys. Rev. A 76 (2007) 031806, http://dx.doi.org/10.1103/PhysRevA.76.031806.
[56] N. Korolkova, G. Leuchs, R. Loudon, T.C. Ralph, C. Silberhorn, Polarization squeezing and continuous-variable polarization entanglement, Phys. Rev. A 65 (2002) 052306, http://dx.doi.org/10.1103/PhysRevA.65.052306.
[57] N.B. An, K. Kim, J. Kim, Generation of cluster-type entangled coherent states using weak nonlinearities and intense laser beams, Quantum Inf. Comput. 11 (1) (2011) 124–141.
[58] Y. Israel, L. Cohen, X.-B. Song, J. Joo, H.S. Eisenberg, Y. Silberberg, Entangled coherent states created by mixing squeezed vacuum and coherent light, Optica 6 (6) (2019) 753–757, http://dx.doi.org/10.1364/OPTICA.6.000753.
[59] H. Takahashi, K. Wakui, S. Suzuki, M. Takeoka, K. Hayasaka, A. Furusawa, M. Sasaki, Generation of large-amplitude coherent-state superposition via ancilla-assisted photon subtraction, Phys. Rev. Lett. 101 (2008) 233605, http://dx.doi.org/10.1103/PhysRevLett.101.233605.
[60] T. Gerrits, S. Glancy, T.S. Clement, B. Calkins, A.E. Lita, A.J. Miller, A.L. Migdall, S.W. Nam, R.P. Mirin, E. Knill, Generation of optical coherent-state superpositions by number-resolved photon subtraction from the squeezed vacuum, Phys. Rev. A 82 (2010) 031802, http://dx.doi.org/10.1103/PhysRevA.82.031802.
[61] C. Gerry, P. Knight, Introductory Quantum Optics, Cambridge University Press, Cambridge, 2004, http://dx.doi.org/10.1017/CBO9780511791239.
[62] A.P. Lund, H. Jeong, T.C. Ralph, M.S. Kim, Conditional production of superpositions of coherent states with inefficient photon detection, Phys. Rev. A 70 (2004) 020101, http://dx.doi.org/10.1103/PhysRevA.70.020101.
[63] P.G. Kwiat, K. Mattle, H. Weinfurter, A. Zeilinger, A.V. Sergienko, Y. Shih, New high-intensity source of polarization-entangled photon pairs, Phys. Rev. Lett. 75 (1995) 4337–4341, http://dx.doi.org/10.1103/PhysRevLett.75.4337.
[64] D.V. Sychev, A.E. Ulanov, A.A. Pushkina, M.W. Richards, I.A. Fedorov, A.I. Lvovsky, Enlargement of optical Schrödinger's cat states, Nat. Photonics 11 (6) (2017) 379–382, http://dx.doi.org/10.1038/nphoton.2017.57.
[65] S. Barz, G. Cronenberg, A. Zeilinger, P. Walther, Heralded generation of entangled photon pairs, Nat. Photonics 4 (8) (2010) 553–556, http://dx.doi.org/10.1038/nphoton.2010.156.
[66] C. Wagenknecht, C.-M. Li, A. Reingruber, X.-H. Bao, A. Goebel, Y.-A. Chen, Q. Zhang, K. Chen, J.-W. Pan, Experimental demonstration of a heralded entanglement source, Nat. Photonics 4 (8) (2010) 549–552, http://dx.doi.org/10.1038/nphoton.2010.123.
[67] L.-K. Chen, H.-L. Yong, P. Xu, X.-C. Yao, T. Xiang, Z.-D. Li, C. Liu, H. Lu, N.-L. Liu, L. Li, T. Yang, C.-Z. Peng, B. Zhao, Y.-A. Chen, J.-W. Pan, Experimental nested purification for a linear optical quantum repeater, Nat. Photonics 11 (11) (2017) 695–699, http://dx.doi.org/10.1038/s41566-017-0010-6.
[68] A.E. Lita, A.J. Miller, S.W. Nam, Counting near-infrared single-photons with 95% efficiency, Opt. Express 16 (5) (2008) 3032–3040, http://dx.doi.org/10.1364/OE.16.003032.
[69] D.H. Smith, G. Gillett, M.P. de Almeida, C. Branciard, A. Fedrizzi, T.J. Weinhold, A. Lita, B. Calkins, T. Gerrits, H.M. Wiseman, S.W. Nam, A.G. White, Conclusive quantum steering with superconducting transition-edge sensors, Nature Commun. 3 (1) (2012) 625, http://dx.doi.org/10.1038/ncomms1628.
[70] J. Borregaard, M. Zugenmaier, J.M. Petersen, H. Shen, G. Vasilakis, K. Jensen, E.S. Polzik, A.S. Sørensen, Scalable photonic network architecture based on motional averaging in room temperature gas, Nature Commun. 7 (1) (2016) 11356, http://dx.doi.org/10.1038/ncomms11356.
[71] T. Heindel, A. Thoma, M. von Helversen, M. Schmidt, A. Schlehahn, M. Gschrey, P. Schnauber, J.H. Schulze, A. Strittmatter, J. Beyer, S. Rodt, A. Carmele, A. Knorr, S. Reitzenstein, A bright triggered twin-photon source in the solid state, Nature Commun. 8 (1) (2017) 14870, http://dx.doi.org/10.1038/ncomms14870.